RESEARCH PAPER

Hispaglabridin B, a constituent of liquorice identified by a bioinformatics and machine learning approach, relieves protein-energy wasting by inhibiting forkhead box O1

Correspondence Lu Lu and Shao-Xiang Xian, The First Affiliated Hospital, Guangzhou University of Chinese Medicine, No. 12 Airport Road, Baiyun District, Guangzhou 510407, China. E-mail: coinland@gzucm.edu.cn; shaoxiangx@hotmail.com

Zeng-Yan Huang[1,2,*], Ling-Jun Wang[1,2,*], Jia-Jia Wang[1,2,*], Wen-Jun Feng[1], Zhong-Qi Yang[1,2], Shi-Hao Ni[1,2], Yu-Sheng Huang[1,2], Huan Li[1,2], Yi Yang[1,2], Ming-Qing Wang[3,4], Rong Hu[3], Heng Wan[5], Chan-Juan Wen[6], Shao-Xiang Xian[1,2] and Lu Lu[1,2] (iD)

[1]*The First Affiliated Hospital, Guangzhou University of Chinese Medicine, Guangzhou, China,* [2]*Lingnan Medical Research Center, Guangzhou University of Chinese Medicine, Guangzhou, China,* [3]*School of Traditional Chinese Medicine, Southern Medical University, Guangzhou, China,* [4]*Peninsula School of Medicine, University of Plymouth, Plymouth, UK,* [5]*Department of Endocrinology, The Third Affiliated Hospital of Southern Medical University, Guangzhou, China, and* [6]*Department of Radiology, Nan Fang Hospital of Southern Medical University, Guangzhou, China*

*These authors contributed equally to this work.

BACKGROUND AND PURPOSE
Liquorice is the root of *Glycyrrhiza glabra*, which is a popular food in Europe and China that has previously shown benefits for skeletal fatigue and nutrient metabolism. However, the mechanism and active ingredients remain largely unclear. The aim of this study was to investigate the active ingredients of liquorice for muscle wasting and elucidate the underlying mechanisms.

EXPERIMENTAL APPROACH
RNA-Seq and bioinformatics analysis were applied to predict the main target of liquorice. A machine learning model and a docking tool were used to predict active ingredients. Isotope labelling experiments, immunostaining, Western blots, qRT-PCR, ChIP-PCR and luciferase reporters were utilized to test the pharmacological effects *in vitro* and *in vivo*. The reverse effects were verified through recombination-based overexpression.

KEY RESULTS
The liposoluble constituents of liquorice improved muscle wasting by inhibiting protein catabolism and fibre atrophy. We further identified FoxO1 as the target of liposoluble constituents of liquorice. In addition, hispaglabridin B (HB) was predicted as an inhibitor of FoxO1. Further studies determined that HB improved muscle wasting by inhibiting catabolism *in vivo* and *in vitro*. HB also markedly suppressed the transcriptional activity of FoxO1, with decreased expression of the muscle-specific E3 ubiquitin ligases MuRF1 and Atrogin-1.

CONCLUSIONS AND IMPLICATIONS
HB can serve as a novel natural food extract for preventing muscle wasting in chronic kidney disease and possibly other catabolic conditions.

Abbreviations
CKD, chronic kidney disease; FoxO, forkhead box O; GSEA, gene set enrichment analysis; MuRF-1, muscle RING-finger 1; NN, neural network; PEW, protein-energy wasting; RF, random forest; SVM, support vector machine

Introduction

Protein-energy wasting (PEW) is one of the most common complications in patients with chronic kidney disease (CKD), which has become a worldwide epidemic, with an incidence of approximately 5–15% in the general population (De Nicola and Zoccali, 2016). An imbalance between protein anabolic and catabolic rates is responsible for muscle wasting (Attaix et al., 2012). Protein catabolism is induced by at least four major proteolytic pathways [lysosomal (Moore and Viarengo, 1987), Ca^{2+}-dependent (Zeman et al., 1986), caspase-dependent (Du et al., 2005) and ubiquitin/proteasome-dependent (Glass, 2003)], while a low protein anabolic rate is commonly attributed to attenuated mTOR signalling (Yoon, 2017). These aspects of protein metabolic signalling may be regarded as potential therapeutic targets for CKD-related muscle wasting.

Forkhead box O (FoxO) proteins are transcriptional factors that play critical roles in the regulation of skeletal muscle mass (Bois and Grosveld, 2003) and control myogenic differentiation and fibre type specification (Kitamura et al., 2007). Four FoxO family members (FoxO1, FoxO3a, FoxO4 and FoxO6) are expressed in mammalian skeletal muscles and two of those proteins, FoxO1 and FoxO3, are key factors in muscle energy homeostasis. The IGF-1/PI3K/Akt pathway critically mediates FoxO inhibition since phosphatidylinositol 3-kinase (PI3K) increases Akt phosphorylation and then phosphorylates and blocks FoxO protein translocation to the nucleus (Glass, 2010). Active FoxO1 or FoxO3 triggers protein degradation via the transcription of the ubiquitin-associated gene muscle atrophy Atrogin-1 (Gomes et al., 2001) and the muscle-specific E3 ubiquitin ligase. muscle RING-finger 1 (MuRF-1) and further initiates the ubiquitin-proteasome pathway. The increase of MuRF1 and Atrogin-1 expression can be blocked through the negative regulation of FoxO transcription factors in several models of skeletal muscle atrophy in both rodents and humans (de Palma et al., 2008). Therefore, FoxO factors may be regarded as a potential drug target to combat muscle wasting. However, until now, no relevant, targeted, drugs have emerged.

Earlier, we focused on the discovery of new drugs to treat PEW and discovered some natural products (Astragalus polysaccharide and ligustilide) that have therapeutic effects on CKD-PEW through modulating protein anabolic and catabolic rates (Shi et al., 2014; Huang et al., 2016; Lu et al., 2016). Liquorice is the root of Glycyrrhiza glabra, which is a popular food plant in Europe and China. Several previous studies have shown that liquorice can improve nutrient metabolism and benefit disorders such as visceral adiposity, diabetes mellitus and dyslipidaemia (Eu et al., 2010; Jungbauer and Medjakovic, 2014; Sil and Chakraborti, 2016). In China, liquorice flavouring is found in a wide variety of candies and sweets and is used in treatments for fatigue and protein wasting (Kao et al., 2014). However, the active compounds and the mechanism of liquorice remain largely unclear. Therefore, the aim of our study was to investigate the main targets and active ingredients of liquorice, as illustrated in Figure S1. In addition, this approach may facilitate the development of more effective strategies to optimize protein nutrition and improve outcomes in CKD patients with PEW.

Methods

Animal experiments

All animal care and experimental procedures complied with the Guidelines for the Care and Use of Laboratory Animals formulated by the Ministry of Science and Technology of China, and were approved by the Ethics Committee of Southern Medical University (approval number: L2015069). Animal studies are reported in compliance with the ARRIVE guidelines (Kilkenny et al., 2010; McGrath and Lilley, 2015). Six-week-old male C57BL/6 mice [obtained from the Experimental Animal Center of Southern Medical University, China, certification no. SCXK (Yue) 2015-0167] weighing 20 ± 1 g were housed in an individual ventilated cage system. All animals were housed at an ambient temperature of 21°C under a 12/12 h light–dark schedule (lights off at 07:00 h) and maintained on food formulated according to the American Institute of Nutrition for Rodent Diets, with ad libitum access to water. The animals were allowed to adapt to their surroundings for 1 week. Randomization was used to assign samples to the experimental groups for all in vivo studies. Data collection and evaluation of all in vivo and in vitro experiments were performed in a blinded manner.

Animal experiments were performed as described in our previous studies (Wang et al., 2014; Lu et al., 2016). Male mice were randomly assigned to either the 5/6 nephrectomised group or the sham-operated group. Surgical plane anaesthesia, as indicated by the Guidelines for the Care and Use of Laboratory Animals, was induced before any surgery was performed. We used a small animal anaesthesia machine (Shenzhen RWD Life Science Co., Ltd, Shenzhen, China) with isoflurane. For induction of anaesthesia, the concentration was 3% and the maintenance concentration was 1.5%. After surgery, mice were placed in a recovery area with thermal support until fully recovered.

Each animal in the nephrectomised group (NPX) underwent a 5/6 nephrectomy, consisting of the ablation of two-thirds of the mass of the left kidney, followed by right unilateral nephrectomy after 1 week. In the sham-operated mice, a sham operation was performed as described earlier (Wang et al., 2014; Lu et al., 2016). The liposoluble extract of liquorice (see Materials for preparation; 0.4 mL each time by gavage, concentrations are shown as mg dry extract per mL vehicle in the Figures 1A) or hispaglabridin (HB; 30 mg·kg^{-1}, i.p.) was administered every 2 days for 18 weeks.

C2C12 myotube differentiation and culture

Cell culture was performed according our previous protocol (Lu et al., 2013; Lu et al., 2016). C2C12 myoblasts were purchased from the Type Culture Collection of the Chinese Academy of Sciences (Shanghai, China). The cells were cultured in high-glucose DMEM containing 10% FBS, 2 mM glutamine, 100 unit·mL^{-1} penicillin and 100 g·mL^{-1} streptomycin. The cells were maintained at 37°C under 5% CO_2 (v/v) in a humidified incubator. The differentiation of myoblasts into myotubes was induced when the cells had achieved 80% confluence by replacing the medium with DMEM

A

B

C

D
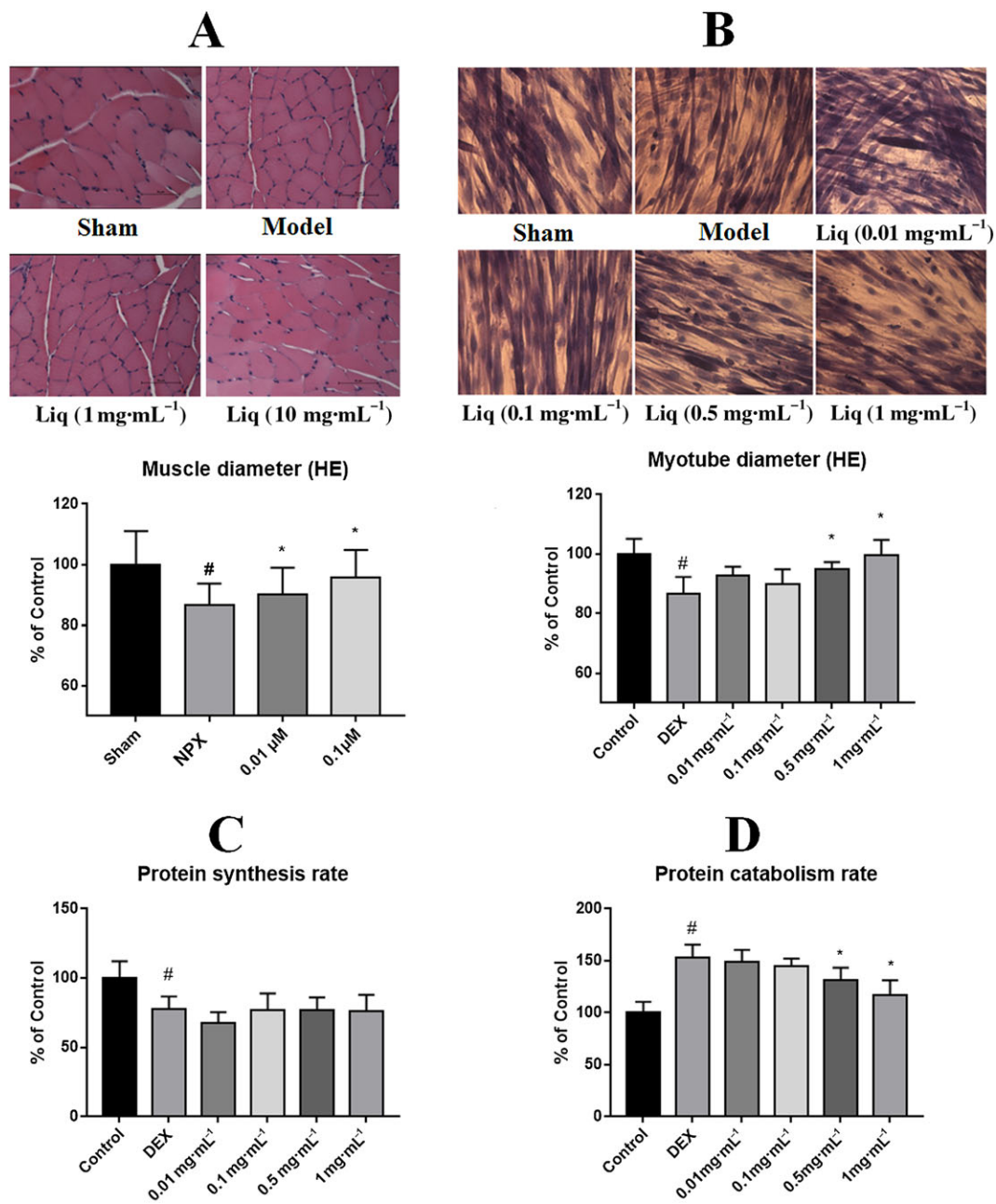
Figure 1

The effect of liposoluble extracts of liquorice on muscle fibres *in vivo* and *in vitro*. (A) H&E staining of the gastrocnemius tissue and quantitative diameter in sham and 5/6 nephrectomised (Model) mice with or without liquorice extract (Liq) treatment (magnification, 200×, n = 400 fibres per group). (B) H&E staining of C2C12 myotubes and quantitative diameter in liquorice extract concentration gradients with or without dexamethasone treatment (magnification, 200×, n = 600 per group). Effect of liquorice liposoluble extracts on the protein synthesis rate (C) and protein catabolism rate (D) in C2C12 myotubes after treatment with different concentrations of extract (n = 6 per group). [#]$P<0.05$, significantly different from control; *$P<0.05$, significantly different from NPX/DEX. DEX, dexamethasone.

containing 2% horse serum. Five to 7 days later, the differentiated myotubes (80% differentiated) were used for experiments.

Myofibre area measurements

Myofibre cross-sectional area and C2C12 fibre size measurements were performed according to previous experiments (Lu *et al.*, 2013). Skeletal muscle samples were fixed in

paraformaldehyde and embedded in paraffin. The muscle samples were sectioned and stained with haematoxylin and eosin (H&E) (or GFP vector transfection for C2C12) according to previously described methods (Lu *et al.*, 2013). The muscle fibre cross-sectional area was measured in a blinded fashion on coded pictures and the investigator analysing the image was unaware of the treatment group. In each muscle, six sections of 50 contiguous myofibres were demarcated so that the

averages of 200 fibres were obtained for the fibre area measurement in each group. Using the Image Pro-Plus software (Media Cybernetics, Bethesda, MD, USA), the borders were delineated with a calibrated pen by circling each fibre. Each fibre was further traced with a handheld mouse to measure the area in pixels and mm.

Dry weight and protein synthesis/degradation

Gastrocnemius muscle samples (for biomolecular detection) and soleus muscle (for protein metabolism detection) were dried in an incubator at 65°C for at least 24 h until the weight remained stable. Then, the weight of every sample was measured. Protein synthesis/degradation rates were measured using our previous protocol (Wang *et al.*, 2014). Protein synthesis was measured *in vitro* in the soleus muscle using the incorporation of phenylalanine, while protein degradation was measured using tyrosine release from the isolated muscle.

RNA-Seq and gene set enrichment analysis (GSEA)

Total mRNA was extracted from the gastrocnemius muscle using an RNA extraction kit (Qiagen K.K., Tokyo, Japan). RNA-Seq was performed using an Ion Proton system for next-generation sequencing, according to the manufacturer's instructions. Sequenced reads were mapped to the mm9 genome using the Ion Torrent TMAP aligner with the 'map 4' option. The RNA-Seq reads that were aligned against the exon regions of genes were quantified with HTSeq-Count in the RefSeq mm9 annotation. GSEA was performed on mRNA expression datasets using the Kyoto Encyclopedia of Genes and Genomes (KEGG) database. Gene signatures were considered enriched if the false discovery rate (FDR) *q*-values and the family-wise error rate (FWER) *P* values showed significant differences.

Drug target prediction

GSEA and motif discovery were used to predict the targets of liquorice constituents. GSEA was performed on mRNA expression datasets using the C2 curated gene sets and C6 oncogenic signature gene sets (GSEA, Broad Institute). Gene signatures were considered enriched if the FDR and the FWER showed significant differences. Transcription factor motif analysis of co-expressed mRNAs was conducted with the motif discovery tool suit MEME. The promoter sequences of co-expressed mRNAs ranged from −500 to 0 bp. The matrices generated by MEME were then compared with the TRANSFAC database using the DNA-binding motif similarity tool STAMP.

Prediction of low MW inhibitors

We built four machine learning models [Bayesian, random forest (RF), support vector machine (SVM) and neural network (NN)] to predict inhibitors of FoxO1 and verify them by molecular docking. Machine learning was performed and optimized in the R program using the Caret package (The source code is provided in the Supporting Information Data S1). The training set of FoxO1 contained 512 samples and was based on Pubchem Bioassay and a literature search. MACCS keys and electrotopological state indices were used for molecule description through the Rcpi package. The model performance was evaluated by ROC methods after 10-fold cross-validation. Low MW compounds in the liposoluble constituents were identified from two Chinese Medicine databases (Shanghai Institute of Organic Chemistry and Traditional Chinese Medicine Database at Taiwan). Molecular docking was performed by the Vina program (Trott and Olson, 2010). The structural model of FoxO1 (Human) was downloaded from the Protein Data Bank (3CO7, the DNA-binding domain of FoxO1 are identical between humans and mice), and the grid docking site was based on the protein-DNA-binding surface. The result was shown by PyMOL.

Western blotting

The protein concentration was measured using BCA methods. After boiling for 15 min, the lysates with 5× loading buffer were loaded equally on 10% SDS polyacrylamide gels. Following electrophoresis, the proteins were transferred to PVDF membranes at a constant 100 V for 90 min. The PVDF membranes were blocked with 5% BSA for 1 h at RT and probed with the respective primary antibodies [rabbit polyclonal anti-mouse p-FoxO1 (Ser^{253} for mouse, corresponds to Ser^{256} for human) antibody (1:1000), p-FoxO1 (Thr^{24}) antibody (1:1000), p-Akt (Ser^{473}) antibody (1:1000), p-FoxO3a (Ser^{253}) antibody (1:1000), anti-synthetic peptide within human MuRF1 antibody (1:1000, reaction with mouse), rabbit monoclonal anti-human Atrogin-1 (1:1000, reaction with mouse)]. A mouse monoclonal anti-mouse GAPDH antibody (1:5000) was used at 4°C overnight. After three washes (15 min each) with PBST, the PVDF membranes were incubated with a HRP-conjugated secondary antibody (1:10000) for 1 h. Finally, after washing with PBST, the blots on the membranes were visualized with an enhanced chemiluminescence (ECL) reagent using a CCD system (ImageStation 2000 MM, Kodak, NY, USA).

Immunohistochemistry and immunofluorescence

The tissue samples were dissected, fixed in 4% paraformaldehyde and sliced into 4 mm paraffin-embedded pieces. After de-waxing, non-specific peroxidase activity was blocked with 3% H_2O_2 for 15 min, followed by three 5 min washes with PBS. The sections were then incubated in 5% BSA-PBS for 30 min and probed with the respective primary antibodies (anti-MuRF-1, 1:100, and anti-Atrogin-1, 1:250; Abcam, Cambridge, UK) at 4°C overnight. Immunostaining with HRP-conjugated secondary antibodies was then performed for 4 h at room temperature.

Cells growing on a glass slide with a confluence of approximately 80% were fixed with 4% paraformaldehyde for 15 min, permeabilized with 0.25% Triton X-100 for 10 min at room temperature and blocked with PBST for 30 min. After washing with PBS, the cells were incubated with a fluorescence-labelled anti-β-catenin antibody (1:200, Abcam). The fluorescence signals were observed using a Leica inverted fluorescence microscope (Leica, Germany).

Real-time fluorescence quantitative PCR

Total RNA was extracted from cells using the TRIzol method (Life Technologies, USA). cDNA was synthesized using the

cDNA Synthesis Supermix for qPCR (Cat. AT341-01, Transgen, Beijing, China) following the manufacturer's instructions. PCR amplification was performed in a reaction volume of 20 μL containing SYBR Green on a thermal cycler (Applied Biosystems 7500, Thermo Fisher Scientific Inc., MA, USA). The following conditions were used: 94°C for 30 s, followed by 42 cycles of 94°C for 5 s and 60°C for 34 s. The data were calculated using the $2^{-\Delta\Delta Ct}$ method (Livak and Schmittgen, 2001), and the primers used are listed below:

5′-TCCTGGATTCCAGAAGATTCAAC-3′ and 5′-TCAGGG ATGTGAGCTGTGACTT-3′ for Atrogin-1, 5′-ACAACCTCTGCCGGAAGTGT-3′ and 5′-CCGCGGTTGGT CCAGTAG-3′ for MuRF1 and 5′-GGATGCAGGGATGATGTTC-3′ and 5′-TGAACCACCAC CTGCTTA-3′ for GAPDH.

Luciferase reporter

For the assay of FoxO1 transcriptional activity, the pGMFOXO-Luc reporter containing multiple FoxO1 motif constructs and the internal control reporter pGME2F-SEAP were obtained from Beijing Biolab Co. (Beijing, China) C2C12 myoblasts were cultured in 24-well plates (1×10^5 cells per well) and co-transfected with 300 ng of pGMFOXO-Luc and 10 ng of pGME2F-SEAP. The cells were lysed at 24 h post-transfection, and luciferase activity was measured with a Dual Luciferase Reporter Assay System (Cat. E1910, Madison, WI, USA).

Chromatin immunoprecipitation (ChIP)-PCR

For ChIP experiments, cells with FoxO1 overexpression were cross-linked with formaldehyde before the chromatin was extracted, sonicated and incubated with primary FoxO1 antibodies or mouse IgG overnight. The antibody complexes were then captured with protein G beads, and the DNA was eluted, de-crosslinked and purified. ChIP signals were calculated by PCR relative to input levels after (IgG) background subtraction. The primers used are listed below:

5′-TCTTGTTTACGACCCCCACG-3′ and 5′-AGGGGACCAGC TGAGCATTC-3′ for the MuRF1 promoter (−195~ −60) and 5′-TCCACGGACGCAAGGTTGTG-3′ and 5′-CACAACCTTGC GTCCGTGGA-3′ for the Atrogin-1 promoter (−150~0).

Lentiviral transfection

The lentivirus vector of the CCD sequence of FoxO1 (CCDS 17343.1, NM_019739.3) was synthesized by Genepharma (Shanghai, China). Target C2C12 myoblasts were infected with lentivirus in the presence of 5 μg·mL^{-1} polybrene. The stable cell lines were established after 1 week of selection with puromycin (1 μg·mL^{-1}), and overexpression of FoxO1 at the protein level was subsequently validated by Western blotting.

Data and statistical analysis

The data and statistical analysis comply with the recommendations on experimental design and analysis in pharmacology (Curtis *et al.*, 2018). Results are expressed as means ± SD. Data were analysed using one-way ANOVA and *post hoc* Tukey's tests were performed only if F achieved the necessary level of statistical significance (GraphPad Prism

6.01; GraphPad Software, Inc., CA, USA). All statistical analyses of bioinformatics data on heatmaps were performed with the R program (3.2, Vienna University of Economics and Business, Austria) and Bioconductor packages (Limma 3.3). Two-sided tests with P values or FDR q-values <0.05 were considered statistically significant for absolute frequency.

Materials

Preparation of liposoluble constituents of liquorice. Liquorice was purchased from the Guangzhou Qingping Medicine Market (Guangzhou, China) and identified by the School of Chinese Traditional Medicine, South Medical University (Guangzhou, China). The liquorice was air-dried, powdered and then extracted with 95% ethanol. For this, 100 g powder was added to 800 mL 95% ethanol and the suspension heated, under reflux at 85°C (water bath) for 2 h. This extraction was repeated twice. The ethanolic extract was evaporated to dryness and stored at −20°C. This dry extract is referred to as the liposoluble constituents of liquorice and the yield of dry ethanolic extract was 8 g obtained from 100 g liquorice powder.

HB was purchased from Chengdu SanHerb Biotech Co. (Chengdu, China). Liposoluble constituents of liquorice and HB were dissolved in a vehicle consisting of DMSO (5% v/v), Tween 80 (1% v/v) and saline (94% v/v) for experimental use.

Nomenclature of targets and ligands

Key protein targets and ligands in this article are hyperlinked to corresponding entries in http://www.guidetopharmacology.org, the common portal for data from the IUPHAR/BPS Guide to PHARMACOLOGY (Harding *et al.*, 2018), and are permanently archived in the Concise Guide to PHARMACOLOGY 2017/18 (Alexander *et al.*, 2017a,b).

Results

Liposoluble extracts of liquorice improved muscle wasting by inhibiting protein catabolism

To test the effects of the liposoluble liquorice extracts on CKD-related PEW, we measured the size of muscle fibres *in vivo* and *in vitro*. Our results showed that the mean cross-sectional area of the gastrocnemius muscle in the NPX group (mice with 5/6 nephrectomy) was nearly 15% lower than that in the Sham group (mice with sham operation). Fibre atrophy was attenuated in the liquorice group compared with that in the NPX group (Figure 1A). *In vitro*, we induced atrophy of C2C12 myotubes *via* **dexamethasone** treatment, which has previously been shown to affect protein metabolism in various ways (Lu *et al.*, 2013, 2016; Yin *et al.*, 2015). Similarly, the diameter of C2C12 myotubes decreased when 1 μM dexamethasone was used (dexamethasone group) and increased when liquorice liposoluble extracts were used at concentrations greater than 0.5 mg·mL^{-1} (Figure 1B). From the isotope labelling experiments, we found that 1 μM dexamethasone inhibited protein synthesis and promoted protein degradation simultaneously. After treatment with a range of concentrations of liposoluble extract, protein synthesis was hardly affected (Figure 1C) but the protein catabolism rate was
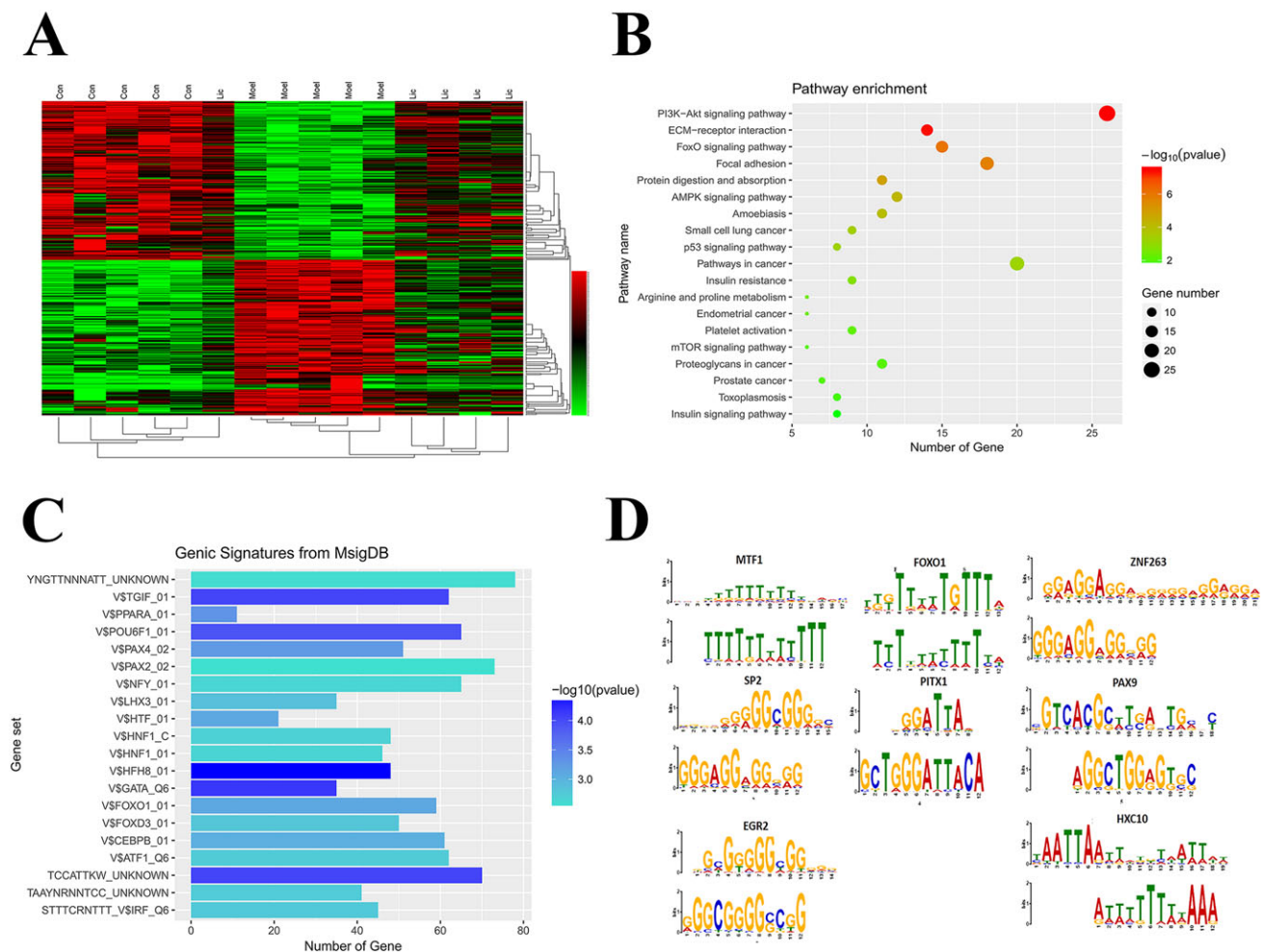
Figure 2

Predicting drug targets of liposoluble liquorice extracts *via* RNA-Seq and bioinformatics analysis. (A) Heatmap and cluster analysis of gene levels for the top 100 differentially expressed genes in the gastrocnemius tissue ($n = 5$ per group). (B) KEGG pathway enrichment analysis of genes in mice with/without liposoluble liquorice extract treatment. The representative pathways include the FoxO signalling pathway. (C) Gene set enrichment analysis in mice with or without liposoluble liquorice extract treatment. (D) Transcription factor binding motifs of co-expressed genes *via* the MEME tool, including FoxO1. (E) The KEGG view of gene expression; the ratios of NPX to Sham (left) and liquorice to NPX (right) are expressed as a colour gradient. (F) Western blot of FoxO1 at two phosphorylation sites (Thr[24] and Ser[253]) in different groups ($n = 5$ per group).
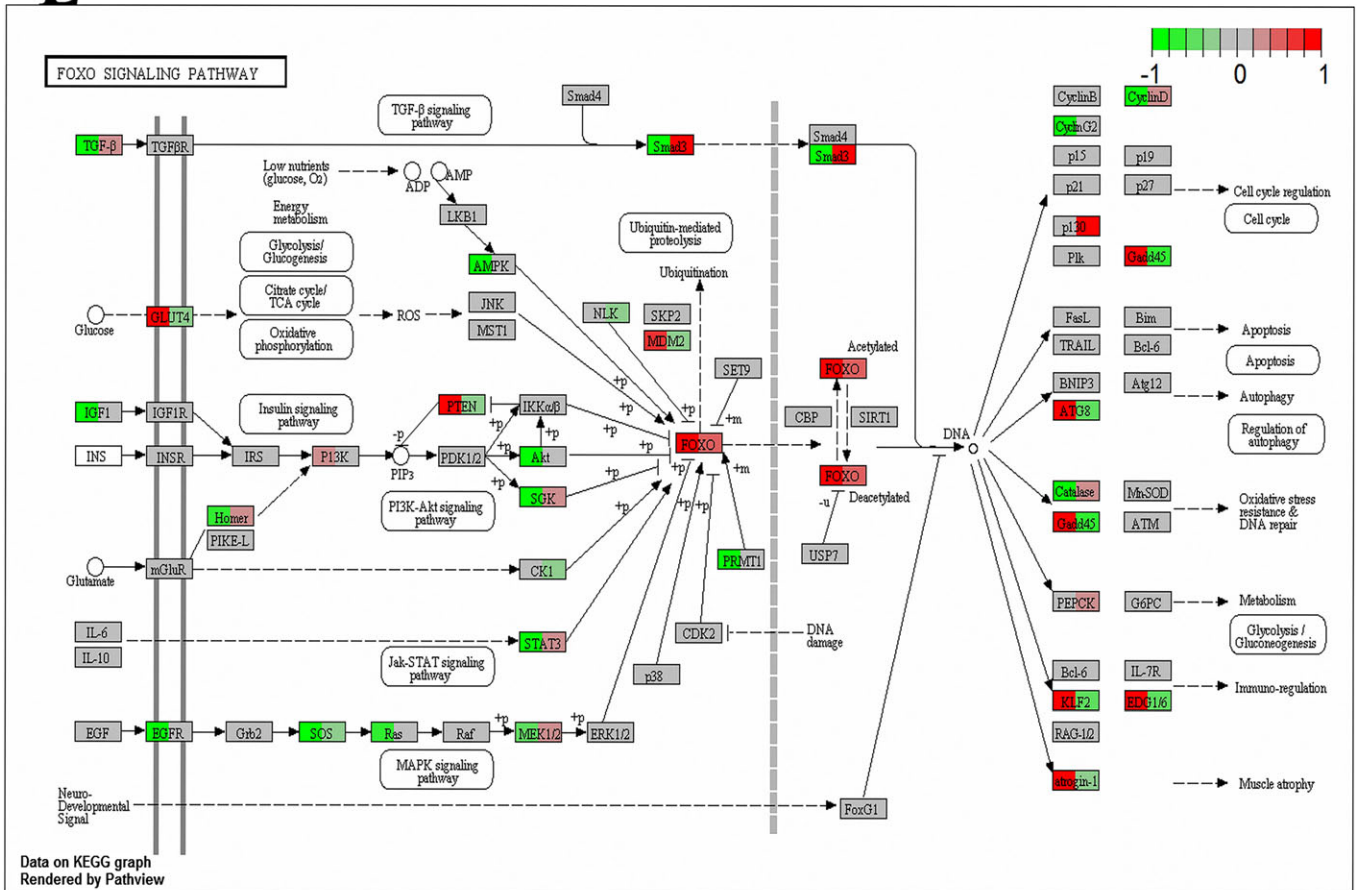
significantly decreased at concentrations greater than 0.5 mg·mL^{-1} (Figure 1D). Collectively, our results show that liposoluble liquorice extracts improved muscle wasting by inhibiting protein catabolism *in vivo* and *in vitro*.

## FoxO1 is the target of liposoluble liquorice extracts

To identify the targets of liquorice extracts, we performed RNA-Seq for each group. The heatmap of the cluster analysis shows that the gene expression patterns were similar in liquorice-treated and sham-treated mice (Figure 2A and Supporting Information Figure S2A), and the results were confirmed by principal component analysis of differentially expressed genes (Supporting Information Figure S2B). Pathway set enrichment from the KEGG database showed that 84 pathways passed the filtering criteria, and 19 representative pathways are shown in Figure 2B. Of those pathways,

the FoxO signalling pathway is closely involved in the protein catabolism rate (Supporting Information Figure S2C). To further verify the target, we performed GSEA for oncogenic signatures in MsigDB, and a total of 44 sets, including 13 genes, passed the filtering criteria, which were considered to be potential downstream targets of liquorice (Figure 2C). We found that FoxO1 passed the filtering criteria (Supporting Information Figure S2D). In addition, motif enrichment based on the MEME Suite tools also showed that the promoter motif of FoxO1 existed in the promoters of co-expressed genes (Figure 2D). The KEGG view of gene expression based on Pathview showed that liquorice extracts reversed the expression of FoxO1-mediated genes (e.g. ATG8, Gadd45, KLF2, EDG1/6 and Atrogin-1) while up-regulating FoxO1 expression (Figure 2E). This finding suggested that liquorice may block FoxO1 in the post-transcriptional phase. Interestingly, Western blots showed that liquorice extracts decreased the phosphorylation of
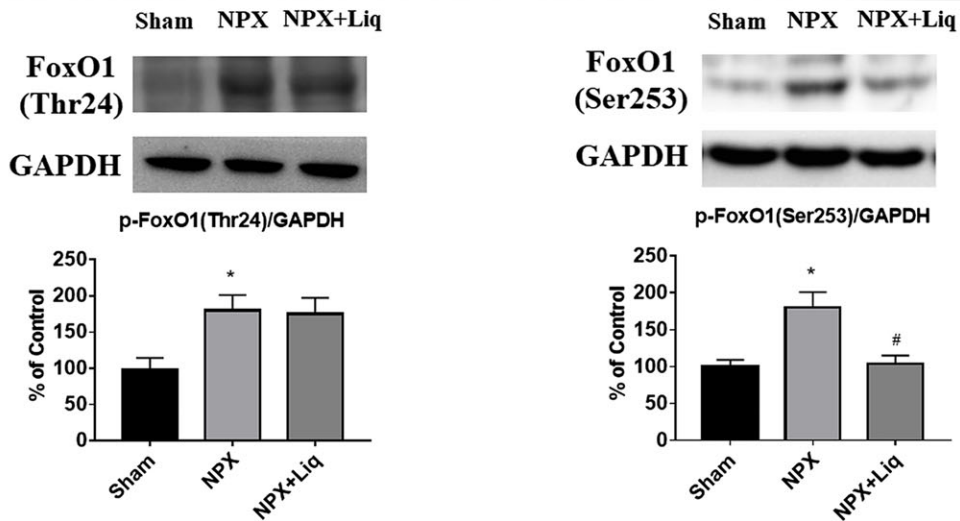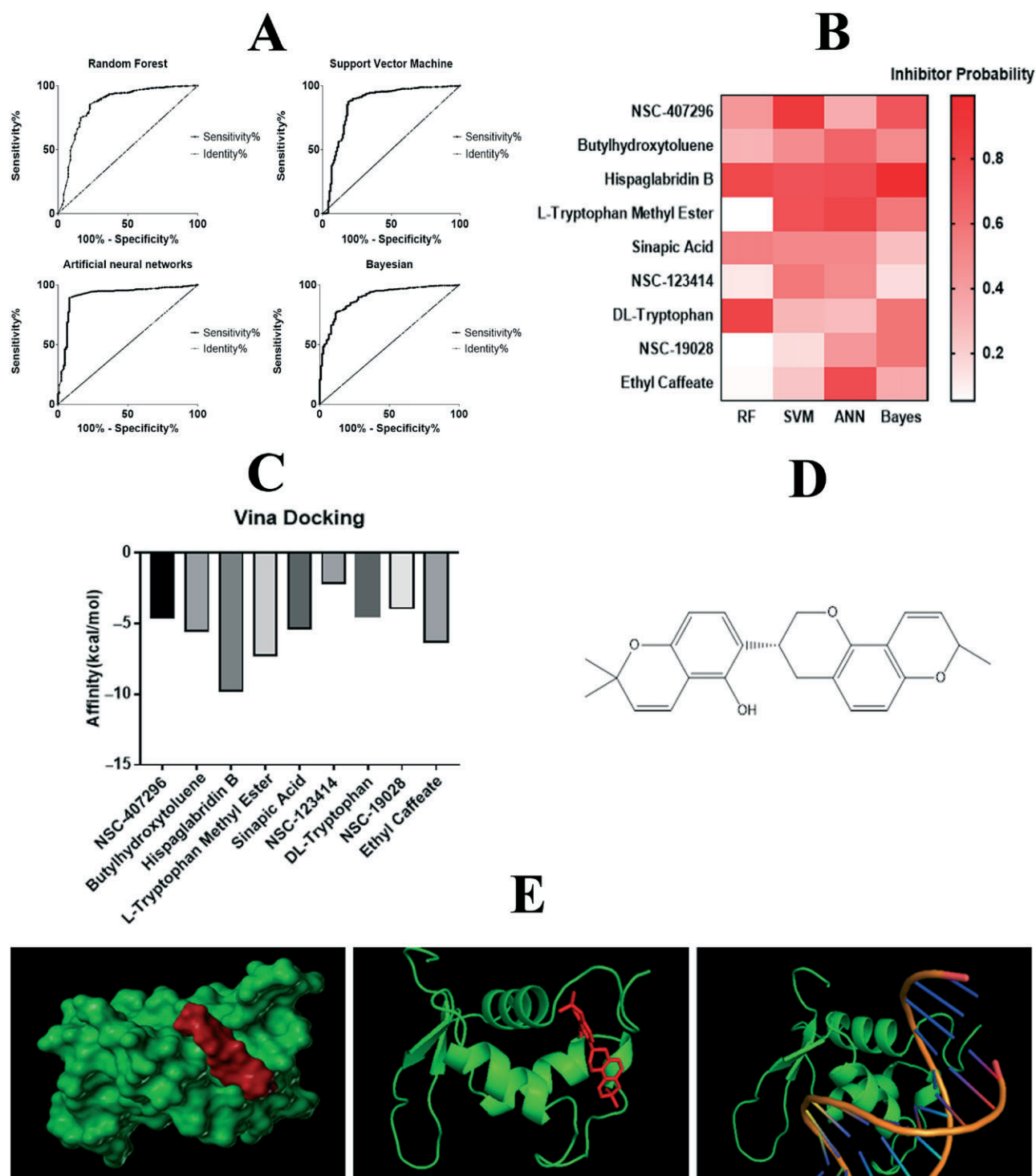
Figure 2

(Continued)

FoxO1 at Ser[253] but had little effect on that at Thr[24], which should promote transcriptional activity (Figure 2F). Given that liquorice actually blocked transcriptional activity, we propose that the extract binds to the active site of FoxO1 and then inhibits its transcriptional activity and phosphorylation simultaneously.

HB is a predicted FoxO1 inhibitor

Next, we aimed to screen for inhibitors of FoxO1. We built four machine learning models (Bayesian, RF, SVM and NN). Model parameters and verification results are shown in Supporting Information Figure S3. From the results of a random 10-fold cross-validation, all area under the ROC
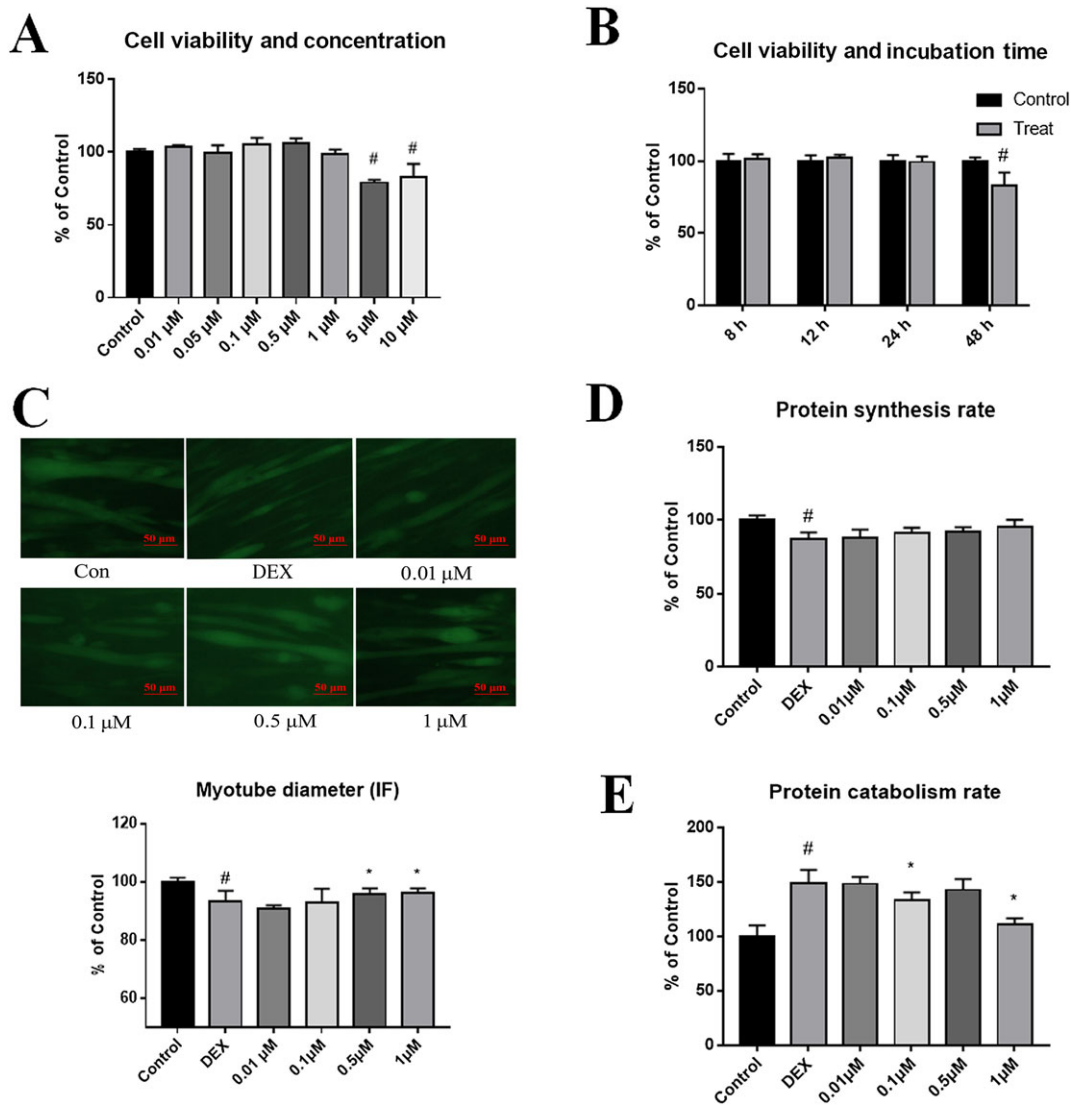
Figure 3

Predicting key active ingredients of liquorice extracts *via* molecular docking and machine learning. (A) ROC curves of four machine learning models (SVM, artificial NN, Bayesian and RF) through 10-fold cross-validation. (B) Heatmap of probability as an inhibitor through four machine learning models. (C) The protein-ligand binding affinity (kcal·mol^{-1}) with applications to molecular docking. (D) The chemical structure of HB. (E) The model of FoxO1 bound to HB with the surface (left), without the surface (middle) and with the DNA-binding site (right).

curve values of our models were greater than 0.76 (Bayesian: 0.838; RF: 0.810; SVM: 0.810 and NN: 0.795, Figure 3A). We identified a molecule as a positive result when

possibility>0.5 from at least two models. After screening for more than 300 compounds by machine learning, 17 compounds from liquorice extracts passed the filtering
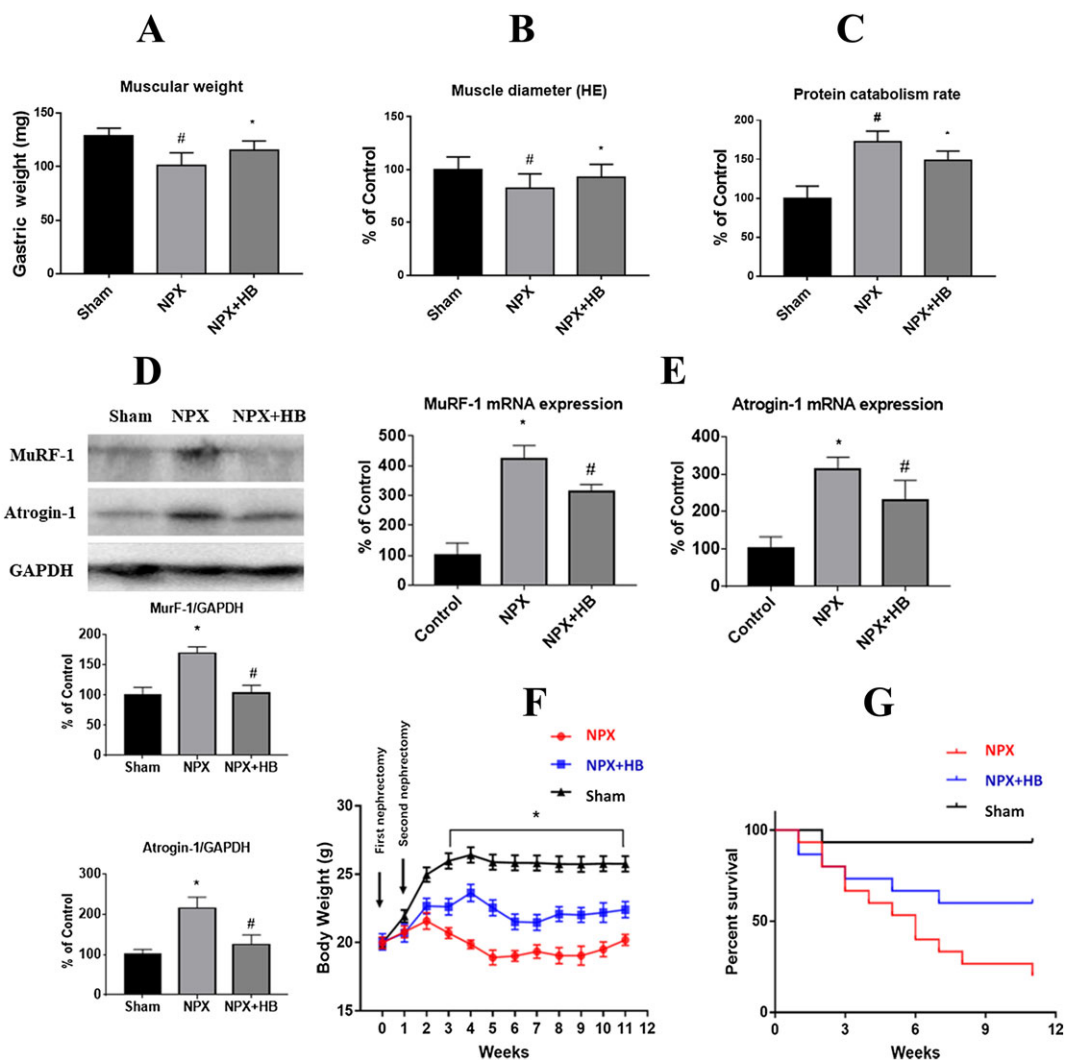
Figure 4

The anti-atrophy effects of HB on C2C12 myotubes. (A) Viability of C2C12 myoblasts incubated with a range of concentrations of HB for 24 h ($n = 8$ per group). (B) Viability of C2C12 myoblasts treated with 0.5 μM HB for the indicated times ($n = 8$ per group). (C) GFP fluorescence of C2C12 myotubes and quantitative diameter, in a range of concentrations of HB (magnification, 200×, $n = 600$ per group). Protein synthesis rate (D) and protein catabolism rate (E) in C2C12 myotubes with different concentrations of HB ($n = 6$ per group). [#]$P<0.05$, significantly different from control; *$P<0.05$, significantly different from DEX. DEX, dexamethasone.

criteria (Figure 3B). To further identify the active compound, we used the Vina docking tool to assess the affinity between the active pocket (DNA-binding region) of FoxO1 and each compound. Of the identified compounds, HB showed the best result (Figure 3C,D). From the docking visualization, HB binds to the pocket of the FoxO1-DNA-binding region, which is near Ser[253] (Figure 3E). This result may explain the dephosphorylating effect of HB.

HB relieves muscle wasting in vivo and in vitro

To explore whether HB can improve protein wasting, we performed experiments *in vivo* and *in vitro*. From the MTT assay, HB did not decrease viability of C2C12 myoblasts until it reached a concentration greater than 5 μM (Figure 4A) or an intervention time greater than 48 h (Figure 4B). The diameter of C2C12 myotubes decreased when 1 μM dexamethasone was used and increased when greater than 0.5 μM HB was used (Figure 4C). From the isotope labelling experiments, HB showed little effect on protein synthesis (Figure 4D) but significantly decreased the protein catabolism rate at concentrations of 0.1 and 1 μM (Figure 4E). After adjusting for cell numbers, HB exhibited an anti-catabolic effect at concentrations ranging from 0.1 to 1 μM (Supporting Information Figure S6). Further animal experiments showed that either the gastrocnemius weight or the muscle diameter increased in mice after HB treatment
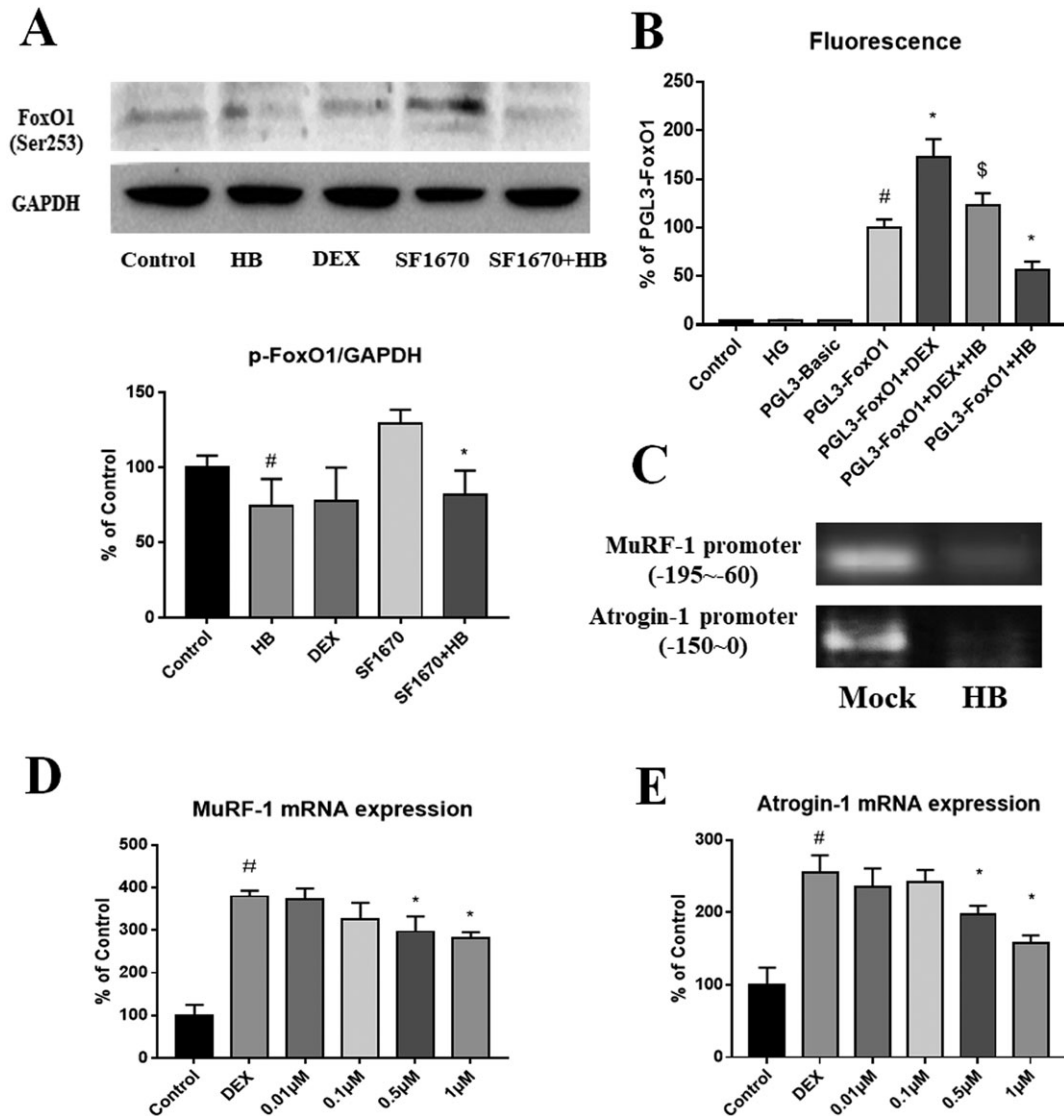
Figure 5

The anti-atrophy effects of HB *in vivo* (*n* = 8 per group). (A) Dry weight of the gastrocnemius in mice with or without HB treatment (*n* = 8 per group). (B) The quantitative diameter of gastrocnemius fibres in different groups (*n* = 400 per group). (C) The protein catabolism rate of the soleus tissue in different groups (*n* = 6 per group). (D) MuRF-1 and Atrogin-1 protein levels in gastrocnemius tissue from mice in different groups (*n* = 5 per group). (E) MuRF-1 and Atrogin-1 mRNA levels in gastrocnemius tissue from mice in different groups (*n* = 8 per group). Change in body weight over 11 weeks of HB intervention (F) and Kaplan–Meier survival curves (G) in sham-treated mice, 5/6 nephrectomised (NPX) mice with HB or equal volume saline treatment (*n* = 15 per group initially). #*P*<0.05, significantly different from control; **P*<0.05, significantly different from NPX.

(Figure 5A,B). The protein catabolism rate significantly decreased compared with that of mice in the NPX group (Figure 5C). Western blotting showed that both MuRF-1 and Atrogin-1 levels increased in the NPX group and these changes were reversed in the HB group (Figure 5D); MuRF-1 and Atrogin-1 mRNA levels were consistent with their protein levels (Figure 5E). In another animal experiment, mice treated with HB showed significantly increased body weight at weeks 3–11 (Figure 5F) and appeared to show increased survival (HR = 0.403, 95% CI = 0.154 to 1.055, Figure 5G), compared with the NPX group.

HB blocked FoxO1 transcriptional activity

To determine whether HB blocked the transcriptional activity of FoxO1, we performed experiments in C2C12 myotubes. SF1670 is a specific **PTEN** inhibitor, which can induce the phosphorylation of Akt (Ser^{473}) and its downstream target FoxO1/3a to inhibit transcription. Western blotting showed that, as reported in Figure 2F, 1 μM HB inhibited FoxO1 phosphorylation at Ser^{253}, with or without SF1670 (for phosphorylating FoxO1) treatment (Figure 6A) but had little effect on Akt (Ser^{473}) and FoxO3a (Thr^{24}, Ser^{253}) phosphorylation, which were also significantly increased by SF1670 treatment (Supporting Information Figure S7). HB decreased the luciferase activity driven by FoxO1 with or without dexamethasone treatment (Figure 6B). ChIP-PCR showed that HB inhibited FoxO1 binding on the promoter motifs of both MuRF-1 and Atrogin-1 (Figure 6C). qRT-PCR showed that the mRNA levels of MuRF-1 and Atrogin-1 decreased significantly after treatment with greater than 0.5 μM HB (Figure 6D,E). Taken

Figure 6

HB blocked FoxO1 transcriptional activity and further decreased MuRF-1/Atrogin-1 levels. (A) Western blot of phosphorylated FoxO1 (Ser[253])/ pan-FoxO1 in C2C12 myotubes with or without dexamethasone, HB and SF1670 ($n = 6$ per group). (B) The luciferase activity driven by the FoxO1 motif was significantly decreased after HB treatment ($n = 6$ per group). (C) Gel electrophoresis of two FoxO1 binding motifs (MuRF-1 and Atrogin-1) *via* ChIP-PCR. (D) mRNA levels of MuRF-1 (D) and Atrogin-1 (E) were significantly decreased after HB treatment compared with the levels observed in the dexamethasone (DEX) group ($n = 8$ per group). [#]$P<0.05$, significantly different from PGL3-Basic; *$P<0.05$, significantly different from PGL3-FoxO1. [$]$P<0.05$, significantly different from PGL3-FoxO1 + DEX.

together, our results show that HB blocked the transcriptional activity of FoxO1.

FoxO1 overexpression reversed HB-induced muscle wasting improvements

To test if FoxO1 is necessary for the HB-induced anti-wasting effect, we used a FoxO1 overexpression model with lentivirus infection. Our results showed that FoxO1 overexpression reversed the anti-atrophy effects of 1 μM HB on C2C12 myotubes (Figure 7A). Immunofluorescence showed that HB restored the myosin heavy chain levels that were decreased by dexamethasone, and the effects were reversed by FoxO1 overexpression (Figure 7B). From the isotope labelling experiments, we found that the protein catabolism rate was decreased through HB treatment and nearly unchanged in cells with FoxO1 overexpression (Figure 7C). qRT-PCR showed that the mRNA levels of both MuRF-1 and Atrogin-1 increased following FoxO1 overexpression (Figure 7D,E). In conclusion, our results demonstrated that HB can relieve muscle wasting *via* the inhibition of FoxO1 (Figure 8).

Discussion

In this study, we found that HB, a constituent of the liposoluble extract of liquorice, pretects against muscle
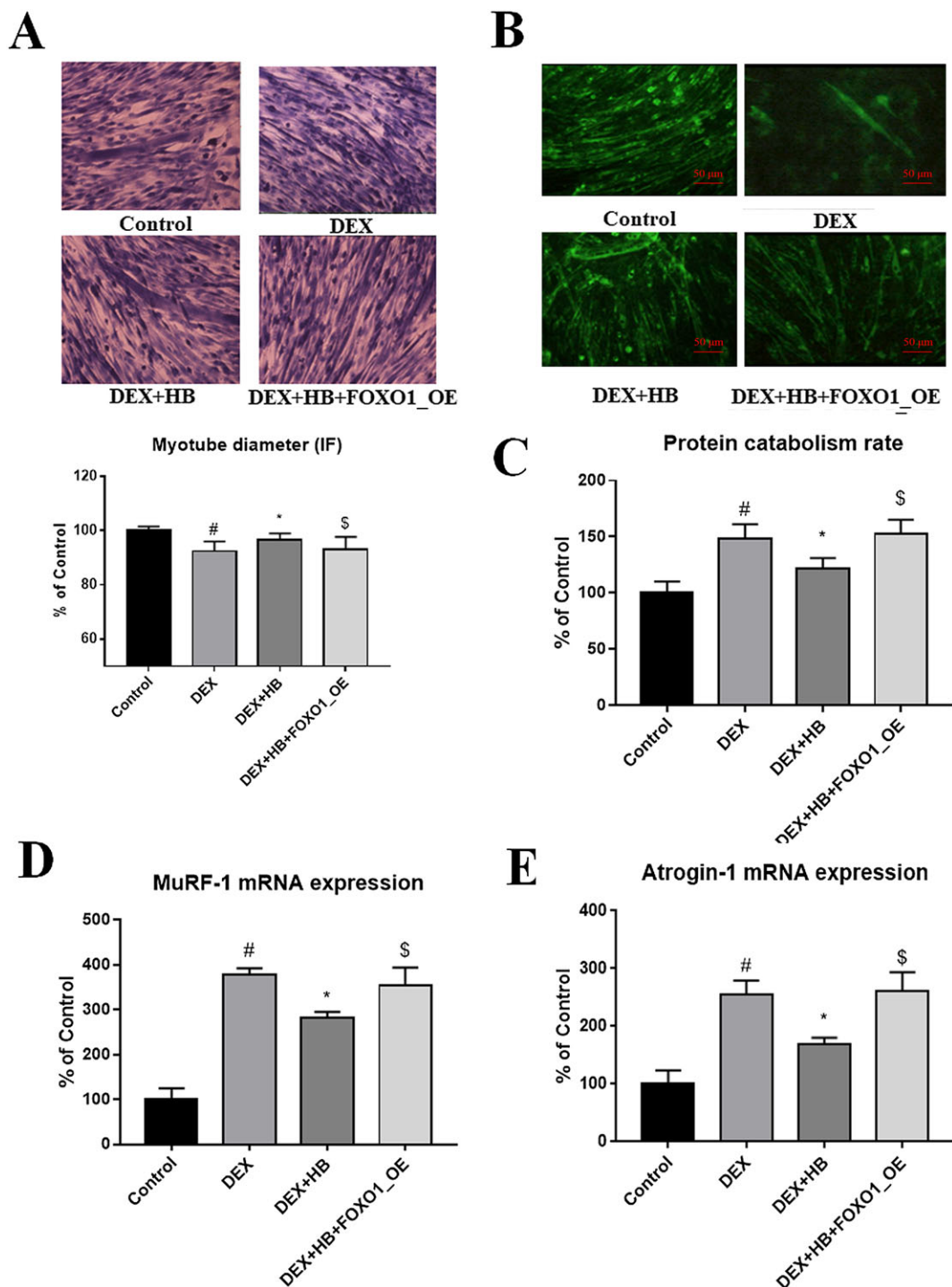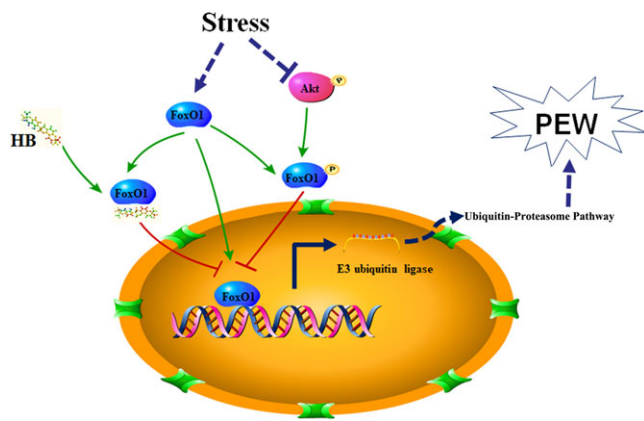
Figure 7

FoxO1 overexpression reverses the anti-atrophy effects of HB. (A) H&E staining of C2C12 myotubes and quantitative diameter with or without dexamethasone/HB treatment (magnification, 200×, $n = 400$ per group). (B) Immunofluorescence of the myosin heavy chain in C2C12 myotubes with or without dexamethasone/HB treatment (magnification, 200×, $n = 6$ per group). (C) The protein catabolism rate of the soleus tissue in different groups ($n = 6$ per group). (D and E) mRNA levels of MuRF-1 and Atrogin-1 in different groups ($n = 8$ per group). [#]$P<0.05$, significantly different from control. *$P<0.05$, significantly different from DEX. [$]$P<0.05$, significantly different from DEX + HB. DEX, dexamethasone.

wasting *via* the inhibition of FoxO1. Notably, we showed that liposoluble liquorice extracts inhibited protein catabolism, which improved muscle atrophy. In addition, our results confirmed that FoxO1 was the target of liposoluble liquorice extracts. We also found that HB was predicted as an inhibitor of FoxO1 by machine learning and molecular docking. Mechanistically, HB prevents muscle wasting *in vivo* and *in vitro* and blocks the transcriptional activity

Figure 8

Diagram of the proposed mechanism by which HB blocks FoxO1 transcriptional activity and reverses PEW.

of FoxO1. To our knowledge, this report is the first to describe the protective effect of HB against skeletal muscle atrophy, and our results provide new insight into FoxO1 as a target for PEW.

The important function of FoxO factors is to regulate two muscle-specific E3 ligases, MuRF1 and MAFbx/Atrogin-1, which are increased transcriptionally in skeletal muscle under atrophy-inducing conditions and to further link the proteasome and protein substrates and initiate the ubiquitin-proteasome pathway (Sandri *et al.*, 2004; Stitt *et al.*, 2004; Waddell *et al.*, 2008; Smith *et al.*, 2010). FoxO1 is a stable protein that continuously shuttles between the nucleus and cytoplasm and depends on cellular metabolic demand to achieve this dynamic equilibrium (Schachter *et al.*, 2012). When FoxO1 is phosphorylated by Akt, this reaction produces a docking site to bind with 14-3-3 proteins, preventing FoxO1 nuclear import (Stitt *et al.*, 2004). These findings demonstrated that the inhibition of muscle wasting requires the blockade of FoxO1, which may be of interest as a potential target to prevent PEW. However, at present, there are no reports of an effective inhibitor of FoxO1 being used for CKD-related PEW. Our study first identified HB as a FoxO1 inhibitor for PEW treatment and confirmed its action in the regulation of FoxO1 transcription factor expression and activity. Interestingly, HB can block the phosphorylation of Ser^{253} and DNA-binding capacity of FoxO1 simultaneously, which suggests that HB acts as a phosphoester at this site. In contrast, previous studies have shown that Glycyrrhiza can reduce body weight by improving glycol-lipid metabolism during the metabolic syndrome (Madak-Erdogan *et al.*, 2016; Yehuda *et al.*, 2016). This observation suggests that liquorice may exert multiple effects on nutritional metabolism, thus meriting further exploration of the specific components and mechanisms. Taken together, our results support an action of HB in preventing the expression of Atrogin-1 and MuRF-1 *via* FoxO1 inhibition, which attenuates protein degradation.

Computer science has been identified as a useful approach to explore drug effectiveness and new compounds with specific features in computer-assisted drug discovery

and design, which greatly increases the efficiency of drug design (Oglic *et al.*, 2018). With the explosive growth of drug data, drug prediction tools such as docking (Barradas-Bautista *et al.*, 2018) and machine learning (de Avila *et al.*, 2017) provide a theoretical framework for the discovery and prioritization of bioactive compounds with desired pharmacological effects and the optimization of those compounds as drug-like leads. In addition, these algorithms are employed to identify the features that may serve to qualitatively or quantitatively distinguish active from inactive compounds (Lavecchia, 2015). To our knowledge, drugs that promote effective resistance to muscle atrophy are still lacking. In the present study, the artificial NN, RF, Bayesian and SVM machine learning methods all suggested that HB had the highest probability of predicted activity and bound to the active pocket of FoxO1 with the highest affinity *via* molecular docking. This molecule was also identified as a FoxO1 phosphorylation inhibitor. Further studies are warranted to investigate the efficacy and safety of this drug and to obtain sufficient evidence from clinical trials.

Importantly, our strategy is not without limitations. Firstly, our machine learning model requires high-quality training datasets. Thus, targets that do not provide ligand data cannot be predicted using our strategy. Second, due to the complex metabolic environment and drug composition *in vivo*, predicting the details of drug metabolism and interaction with biological signals is almost impossible. Therefore, theoretical compound doses may not accurately quantify the corresponding phenotype. Third, herbs and traditional Chinese medicines are considered to have the characteristics of 'multi-components to multi-targets'. Therefore, some ingredients with biological activity *in vivo* may be excluded due to strict screening procedures. In addition, the species of the selected data must be considered for the basis and risks of the model.

In conclusion, our findings reveal an important action of HB in relieving muscle wasting *via* the inhibition of FoxO1 *in vivo* and *in vitro*. HB may serve as a lead compound in the search for a therapeutic agent to preventing muscle wasting through the inhibition of the FoxO1 pathway, and this approach may lead to the generation of novel therapeutic strategies for CKD patients with PEW.

Acknowledgements

Author contributions

H.Z.Y. and W.L.J. initiated the project with guidance from L.L. and X.S.X. Animal studies were performed by F.W.J., Y.Z.Q. and N.S.H. with help from H.Y.S., L.H. and W.J.J. Y.Y., W.M.Q. and H.R. collected the culture medium samples and

measured myotube diameter. Data analysis was primarily performed by H.Z.Y. and W.L.J., aided by W.H., and W.C.J. H.Z.Y. and W.L.J. prepared the figures and wrote the manuscript with input from X.S.X. and L.L. The experiments during revision of the paper were completed by W.J.J.

Conflicts of interest

The authors declare no conflicts of interest.

Declaration of transparency and scientific rigour

This Declaration acknowledges that this paper adheres to the principles for transparent reporting and scientific rigour of preclinical research recommended by funding agencies, publishers and other organisations engaged with supporting research.

References

Alexander SPH, Kelly E, Marrion NV, Peters JA, Faccenda E, Harding SD *et al*. (2017a). The Concise Guide to PHARMACOLOGY 2017/18: Other proteins. Br J Pharmacol 174: S1–S16.

Alexander SPH, Fabbro D, Kelly E, Marrion NV, Peters JA, Faccenda E *et al*. (2017b). The Concise Guide to PHARMACOLOGY 2017/18: Enzymes. Br J Pharmacol 174: S272–S359.

Attaix D, Baracos VE, Pichard C (2012). Muscle wasting: a crosstalk between protein synthesis and breakdown signalling. Curr Opin Clin Nutr Metab Care 15: 209–210.

Barradas-Bautista D, Rosell M, Pallara C, Fernandez-Recio J (2018). Structural prediction of protein-protein interactions by docking: application to biomedical problems. Adv Protein Chem Struct Biol 110: 203–249.

Bois PR, Grosveld GC (2003). FKHR (FOXO1a) is required for myotube fusion of primary mouse myoblasts. EMBO J 22: 1147–1157.

Curtis MJ, Alexander S, Cirino G, Docherty JR, George CH, Giembycz MA *et al*. (2018). Experimental design and analysis and their reporting II: updated and simplified guidance for authors and peer reviewers. Br J Pharmacol 175: 987–993.

de Avila MB, Xavier MM, Pintro VO, de Azevedo WF Jr (2017). Supervised machine learning techniques to predict binding affinity. A study for cyclin-dependent kinase 2. Biochem Biophys Res Commun 494: 305–310.

De Nicola L, Zoccali C (2016). Chronic kidney disease prevalence in the general population: heterogeneity and concerns. Nephrol Dial Transplant 31: 331–335.

de Palma L, Marinelli M, Pavan M, Orazi A (2008). Ubiquitin ligases MuRF1 and MAFbx in human skeletal muscle atrophy. Joint Bone Spine 75: 53–57.

Du J, Hu Z, Mitch WE (2005). Molecular mechanisms activating muscle protein degradation in chronic kidney disease and other catabolic conditions. Eur J Clin Invest 35: 157–163.

Eu CH, Lim WY, Ton SH, bin Abdul Kadir K (2010). Glycyrrhizic acid improved lipoprotein lipase expression, insulin sensitivity, serum

lipid and lipid deposition in high-fat diet-induced obese rats. Lipids Health Dis 9: 81.

Glass DJ (2003). Molecular mechanisms modulating muscle mass. Trends Mol Med 9: 344–350.

Glass DJ (2010). PI3 kinase regulation of skeletal muscle hypertrophy and atrophy. Curr Top Microbiol Immunol 346: 267–278.

Gomes MD, Lecker SH, Jagoe RT, Navon A, Goldberg AL (2001). Atrogin-1, a muscle-specific F-box protein highly expressed during muscle atrophy. Proc Natl Acad Sci U S A 98: 14440–14445.

Harding SD, Sharman JL, Faccenda E, Southan C, Pawson AJ, Ireland S *et al*. (2018). The IUPHAR/BPS guide to pharmacology in 2018: updates and expansion to encompass the new guide to immunopharmacology. Nucl Acids Res 46: D1091–D1106.

Huang YF, Lu L, Zhu DJ, Wang M, Yin Y, Chen DX *et al*. (2016). Effects of astragalus polysaccharides on dysfunction of mitochondrial dynamics induced by oxidative stress. Oxid Med Cell Longev 2016: 9573291.

Jungbauer A, Medjakovic S (2014). Phytoestrogens and the metabolic syndrome. J Steroid Biochem Mol Biol 139: 277–289.

Kao TC, Wu CH, Yen GC (2014). Bioactivity and potential health benefits of licorice. J Agric Food Chem 62: 542–553.

Kilkenny C, Browne W, Cuthill IC, Emerson M, Altman DG (2010). Animal research: reporting in vivo experiments: the ARRIVE guidelines. Br J Pharmacol 160: 1577–1579.

Kitamura T, Kitamura YI, Funahashi Y, Shawber CJ, Castrillon DH, Kollipara R *et al*. (2007). A Foxo/Notch pathway controls myogenic differentiation and fiber type specification. J Clin Invest 117: 2477–2485.

Lavecchia A (2015). Machine-learning approaches in drug discovery: methods and applications. Drug Discov Today 20: 318–331.

Livak KJ, Schmittgen TD (2001). Analysis of relative gene expression data using real-time quantitative PCR and the $2-\Delta\Delta CT$ method. Methods 25: 402–408.

Lu L, Huang YF, Chen DX, Wang M, Zou YC, Wan H *et al*. (2016). Astragalus polysaccharides decrease muscle wasting through Akt/mTOR, ubiquitin proteasome and autophagy signalling in 5/6 nephrectomised rats. J Ethnopharmacol 186: 125–135.

Lu L, Wang DT, Shi Y, Yin Y, Wei LB, Zou YC *et al*. (2013). Astragalus polysaccharide improves muscle atrophy from dexamethasone- and peroxide-induced injury in vitro. Int J Biol Macromol 61: 7–16.

Madak-Erdogan Z, Gong P, Zhao YC, Xu L, Wrobel KU, Hartman JA *et al*. (2016). Dietary licorice root supplementation reduces diet-induced weight gain, lipid deposition, and hepatic steatosis in ovariectomized mice without stimulating reproductive tissues and mammary gland. Mol Nutr Food Res 60: 369–380.

McGrath JC, Lilley E (2015). Implementing guidelines on reporting research using animals (ARRIVE etc.): new requirements for publication in BJP. Br J Pharmacol 172: 3189–3193.

Moore MN, Viarengo A (1987). Lysosomal membrane fragility and catabolism of cytosolic proteins: evidence for a direct relationship. Experientia 43: 320–323.

Oglic D, Oatley SA, Macdonald SJF, McInally T, Garnett R, Hirst JD *et al*. (2018). Active search for computer-aided drug design. Mol Inform 37.

Sandri M, Sandri C, Gilbert A, Skurk C, Calabria E, Picard A *et al*. (2004). FoxO transcription factors induce the atrophy-related ubiquitin ligase atrogin-1 and cause skeletal muscle atrophy. Cell 117: 399–412.

Schachter TN, Shen T, Liu Y, Schneider MF (2012). Kinetics of nuclear-cytoplasmic translocation of FoxO1 and FoxO3A in adult skeletal muscle fibers. Am J Physiol Cell Physiol 303: C977–C990.

Shi Y, Wang D, Lu L, Yin Y, Wang M, Li C *et al*. (2014). Ligustilide prevents the apoptosis effects of tumour necrosis factor-alpha during C2C12 cell differentiation. Int Immunopharmacol 19: 358–364.

Sil R, Chakraborti AS (2016). Oxidative inactivation of liver mitochondria in high fructose diet-induced metabolic syndrome in rats: effect of glycyrrhizin treatment. Phytother Res: PTR 30: 1503–1512.

Smith IJ, Alamdari N, O'Neal P, Gonnella P, Aversa Z, Hasselgren PO (2010). Sepsis increases the expression and activity of the transcription factor forkhead box O 1 (FOXO1) in skeletal muscle by a glucocorticoid-dependent mechanism. Int J Biochem Cell Biol 42: 701–711.

Stitt TN, Drujan D, Clarke BA, Panaro F, Timofeyva Y, Kline WO *et al*. (2004). The IGF-1/PI3K/Akt pathway prevents expression of muscle atrophy-induced ubiquitin ligases by inhibiting FOXO transcription factors. Mol Cell 14: 395–403.

Trott O, Olson AJ (2010). AutoDock Vina: improving the speed and accuracy of docking with a new scoring function, efficient optimization, and multithreading. J Comput Chem 31: 455–461.

Waddell DS, Baehr LM, van den Brandt J, Johnsen SA, Reichardt HM, Furlow JD *et al*. (2008). The glucocorticoid receptor and FOXO1 synergistically activate the skeletal muscle atrophy-associated MuRF1 gene. Am J Physiol Endocrinol Metab 295: E785–E797.

Wang DT, Lu L, Shi Y, Geng ZB, Yin Y, Wang M *et al*. (2014). Supplementation of ketoacids contributes to the up-regulation of the Wnt7a/Akt/p70S6K pathway and the down-regulation of apoptotic and ubiquitin-proteasome systems in the muscle of 5/6 nephrectomised rats. Br J Nutr 111: 1536–1548.

Yehuda I, Madar Z, Leikin-Frenkel A, Szuchman-Sapir A, Magzal F, Markman G *et al*. (2016). Glabridin, an isoflavan from licorice root, upregulates paraoxonase 2 expression under hyperglycemia and protects it from oxidation. Mol Nutr Food Res 60: 287–299.

Yin Y, Lu L, Wang D, Shi Y, Wang M, Huang Y *et al*. (2015). Astragalus polysaccharide inhibits autophagy and apoptosis from peroxide-induced injury in C2C12 myoblasts. Cell Biochem Biophys 73: 433–439.

Yoon MS (2017). mTOR as a key regulator in maintaining skeletal muscle mass. Front Physiol 8: 788.

Zeman RJ, Bernstein PL, Ludemann R, Etlinger JD (1986). Regulation of Ca^{2+}-dependent protein turnover in skeletal muscle by thyroxine. Biochem J 240: 269–272.

Supporting Information

Additional supporting information may be found online in the Supporting Information section at the end of the article.

https://doi.org/10.1111/bph.14508

Data S1 Supporting Information.

Figure S1 Our prediction strategy for identifying targets and active small molecules in effective mixture, based on bioinformatics analysis and machine learning. Briefly, we obtained a full transcriptional profile through RNA-Seq and then predicted the primary targets based on a genetic profile database *via* GSEA. After determining the target, we trained four machine learning models based on the known action components of the target and then predicted the possible targeting components from the mixture *via* a trained machine learning model. Finally, we verified the predictions by molecular biology methods. This study focused on identifying the primary target small molecules of liquorice through our prediction strategy, followed by identification *in vitro* and *in vivo*.

Figure S2 Overall analysis of gene expression from RNA-Seq. (A) Heatmap of dissimilarities between mouse samples based on the Euclidean distances of differentially expressed genes. (B) Principal component analysis (PCA) based on differentially expressed genes. The characters represents the sample numbers. Gene set enrichment analysis (GSEA) for gene signatures of the FoxO pathway (C) and FoxO-related genes (D) in model mice with/without liquorice treatment.

Figure S3 Machine learning models were optimized through repeated cross-validation. The optimal parameters were selected using area under the ROC curve as the train metric: (A) RF (Predictors = 40); (B) SVM (Cost = 1.0); (C) NN (Hidden Units = 5 and Weight Decay = 0.1); (D) Bayesian (Base Terminal Node Hyperparameter = 0.991 and Power Terminal Node Hyperparameter = 2).

Figure S4 Plasma concentration of HB at different times. (A) Typical chromatograms of plasma alone or spiked with HB. (B) The proposed fragment of HB in negative-ion mode and positive-ion mode for mass spectrometry detection. Mean ± SD ($n = 5$) plasma concentration-time profiles of HB following oral administration of 10 mg/mL liquorice extract (0.4 mL per mice) (C) or intraperitoneal administration of 30 mg/kg HB (D).

Figure S5 The effects of liquorice extract and HB alone on C2C12 myotubes. The effect of 0.1 mg/mL and 1 mg/mL liquorice exact on C2C12 myotube diameter (A) and protein catabolism rate (B). The effect of 0.1 μM and 1 μM HB on C2C12 myotube diameter (C) and protein catabolism rate (D). *Significant difference *vs*. control.

Figure S6 Protein catabolism rate in C2C12 myotubes treated with different concentrations of HB. The results were adjusted by nuclear number. *Significant difference *vs*. control; #Significant difference *vs*. DEX.

Figure S7 The effect of SF1670 (PTEN inhibitor) with or without HB treatment on the phosphorylation of Akt at Ser473 (A), FoxO1 at Ser253 and FoxO3a at Thr24 (B). $n = 5$ per group, *Significant difference *vs*. control.

Figure S8 FoxO1 overexpression exerted an atrophy effect on C2C12 myotubes. (A) H&E staining of C2C12 myotubes and quantitative diameter with FoxO1 overexpression (magnification, 200X, $n = 300$ per group). Immunofluorescence of the myosin heavy chain (MHC) in C2C12 myotubes with FoxO1 overexpression (magnification, 200X).